Physics and Chemistry of Minerals (2020) 47:33
https://doi.org/10.1007/s00269-020-01101-x

ORIGINAL PAPER

Effect of pressure on the kinetics of peridotite serpentinization

Ruifang Huang[1] · Weidong Sun[2] · Xing Ding[3] · Yusheng Zhao[1] · Maoshuang Song[3]

Received: 27 February 2020 / Accepted: 23 June 2020

Abstract

The kinetics of serpentinization were investigated at 400–500 °C and 3.0–20 kbar using natural olivine and peridotite for run durations of 9–38 days. The serpentine varieties were lizardite for all the experiments. The serpentinization kinetics at 400 °C and 3.0 kbar and at 500 °C and 20 kbar displayed a sigmoidal kinetic behavior, with very sluggish reaction rates at the early stage of serpentinization, followed by a sudden increase in the reaction rates. They were 1–2 orders of magnitude faster than serpentinization kinetics commonly used for modeling serpentinization-related processes. Pressure greatly increases the rates of peridotite serpentinization at 500 °C, e.g., 19% of reaction extent was achieved within 20 days for experiments at 500 °C and 3.0 kbar with starting grain sizes of < 30 μm, which increased to 96% for experiments at 500 °C and 20 kbar over the same period. Compared to olivine, peridotite was serpentinized at much faster rates at 400–500 °C and 3.0 kbar, reflecting the influence of pyroxene and spinel. Pyroxene minerals released some of its SiO_2 during serpentinization, which was involved in the serpentinization of olivine, supported by larger amounts of SiO_2 in olivine-derived serpentine compared to those of primary olivine. Thermodynamic calculations suggest that Gibbs energy of olivine hydrolysis decreases greatly with increasing pressures, and it becomes negative at 400–500 ºC and 3.0–20 kbar with the involvement of silica. The experimental results of this study may be applied to natural geological settings where abundant H_2O is present.

Keywords Serpentinization kinetics · Pyroxene · Silica · Aluminum

Introduction

A wide range of geological and geophysical evidence suggests that the oceanic lithosphere and the mantle wedge are considerably serpentinized (e.g., Peacock 2001; Hyndman and Peacock 2003; Hirth and Guillot 2013). Serpentinization greatly reduces the strength of the oceanic lithosphere and the mantle wedge (e.g., Escartín et al. 1997, 2001), influences the recycling of H_2O and fluid-mobile elements (e.g., Cs, Rb, and Ba) in subduction zones (e.g., Hattori and Guillot 2003; Scambelluri et al. 2001, 2004; Guillot and Hattori 2013), triggers partial melting in the mantle and arc magmatism (Hattori and Guillot 2003; Guillot and Hattori 2013), and may be related to the formation of oceans (e.g., Wallmann 2001; Rüpke et al. 2004). Serpentine is a hydrous silicate mineral containing up to 13 wt% H_2O and is stable at depths of greater than 150 km (Ulmer and Trommsdorff 1995; Schmidt and Poli 1998). Therefore, serpentine is an important chemical reservoir of H_2O in subduction zones. However, the degree of serpentinized peridotites in the mantle wedge remains poorly constrained (e.g., Iyer et al. 2010, 2012), which is significant for understanding the recycling of water in subduction zones, and the dynamics of the past and present Earth.

Serpentinization kinetics, an essential parameter for quantifying the proportions of serpentine and water in subduction zones (e.g., Iyer et al. 2010, 2012), have been experimentally studied over 50 years mostly at relatively low pressures (≤ 3 kbar) (Martin and Fyfe 1970; Wegner and Ernst

Electronic supplementary material The online version of this article (https://doi.org/10.1007/s00269-020-01101-x) contains supplementary material, which is available to authorized users.

✉ Ruifang Huang
huangrf@sustech.edu.cn

[1] SUSTech Academy for Advanced Interdisciplinary Studies, Southern University of Science and Technology, Shenzhen 518055, People's Republic of China

[2] Center of Deep Sea Research, Institute of Oceanology, Chinese Academy of Sciences, Qingdao 266071, People's Republic of China

[3] State Key Laboratory of Isotope Geochemistry, Guangzhou Institute of Geochemistry, Chinese Academy of Sciences, Guangzhou 510640, People's Republic of China

Published online: 04 July 2020

1983; Seyfried et al. 2007; Marcaillou et al. 2011; Lafay et al. 2012, 2014; Malvoisin et al. 2012; McCollom et al. 2016; Huang et al. 2017a). Until now, only Nakatani and Nakamura (2016) have reported the kinetics of serpentinization by reacting crushed powders of olivine ± orthopyroxene and orthopyroxene + clinopyroxene with distilled water at 400–580 °C and 13–18 kbar, and the kinetics of serpentinization were 3–4 orders of magnitude faster compared to the rates of olivine serpentinization at ≥ 350 °C and relatively low pressures (e.g., ≤ 3.0 kbar) (Malvoisin et al. 2012; McCollom et al. 2016). However, the factors that induce such great contrast, including pressure, temperature, and fluid compositions, are poorly constrained. In this study, we re-investigated the rates of serpentinization at 400–500 °C and 3.0–20 kbar by reacting natural crushed peridotite and olivine with saline solutions (0.5 M NaCl). We found that the rates of peridotite serpentinization at 500 °C increased by around 4 times with increasing pressures from 3.0 to 20 kbar. In particular, the rates of olivine serpentinization at 400–500 °C and 3.0–20 kbar increased significantly with the presence of pyroxene and spinel.

Materials and methods

Preparation of starting materials

The experimental strategy used in this study was to react crushed peridotite and olivine with saline solutions (0.5 mol/L NaCl). The peridotite was sampled at Panshishan (Jiangsu Province, China), where it occurs as xenoliths in alkaline basalts (e.g., Chen et al. 1994; Sun et al. 1998; Xu et al. 2008). The peridotite has a very low loss on ignition, < 0.5% (Yang 2008), which suggests that the sample is fresh without any lateral hydrothermal alteration. The peridotite was composed of ~ 65 vol% olivine, 20 vol% orthopyroxene, 15 vol% clinopyroxene, and 1–2 vol% spinel. More detailed information about the peridotite has been described in previous studies (Huang et al. 2017a, 2019). The sample was disaggregated, ground in an agate mortar and then sieved into starting grain sizes of < 30 μm, 42–59 μm, 86–106 μm, and 100–177 μm. These grains were subsequently cleaned in an ultrasonic bath to remove very fine particles.

Pure olivine grains were picked from crushed peridotite (> 250 μm) under a binocular microscope, and those with the inclusion of other mineral phases were excluded. The grains were then cleaned in an ultrasonic bath to remove very fine particles adhered on the surface of olivine, especially pyroxene and spinel. Mechanical mixtures of olivine and pyroxene minerals (i.e., spinel-free peridotite) were also prepared by removing spinel from crushed peridotite (> 250 μm). Olivine grains and spinel-free peridotite were ground in an agate mortar and sieved into starting grain sizes of < 30 μm. Subsequently, they were washed in an ultrasonic bath to eliminate fine grains. Saline solutions (0.5 mol/L NaCl) were prepared using reagent-grade NaCl and deionized water.

Hydrothermal experiments

All the experiments of this study were performed in a high-pressure laboratory, Guangzhou Institute of Geochemistry, Chinese Academy of Sciences (Table 1). Experiments at 400–500 °C and 3.0 kbar were conducted in cold-seal hydrothermal vessels. The gold capsules (4.0 mm O. D., 3.6 mm I. D. and ~ 30 mm long) with solid reactants (~ 50 mg) and saline solutions (~ 50 mg) were sealed at both ends with a tungsten inert gas high-frequency pulse welder (PUK3), and they were placed at the end of vessels, followed by a filler rod (~ 60 mm long). Water was taken as the pressure medium, and pressure was achieved by pumping water into the vessel and measured by a pressure gauge with a precision of ± 100 bar. Temperature was monitored by an external K-type thermocouple that was inserted into a hole near the end of the vessel. The accuracy of temperature is within ± 2 °C. Quenching was facilitated with immersion into water bath, and temperatures decreased to < 100 °C within 10 s.

Experiments at 500 °C and 8.0–20 kbar were performed in a Quickpress piston-cylinder apparatus (e.g., Xia et al. 2014; Huang et al. 2017b). The assemblies comprised a NaCl sleeve wrapped in lead foil, an outer Pyrex sleeve, a graphite furnace and inner rods of MgO. The gold capsules (3.0 mm O. D., 2.6 mm I. D. and 8 mm long) loaded with solid reactants (~ 30 mg) and saline solutions (~ 10 mg) were encased in an MgO sleeve, and they were sealed at both ends with a tungsten inert gas high-frequency pulse welder (PUK3). Temperature was measured by an S-type thermocouple with a variation of ± 1 °C. Hot piston-out method was taken to pressurize the assembly without friction correction, which is < 8% based on pressure calibration.

Analytical techniques

All the solid experimental products were recovered, and they were analyzed by X-ray diffraction (XRD), Scanning electron microscope (SEM), Fourier transform infrared spectroscopy (FTIR), Raman spectroscopy, and electron microprobe. X-ray diffraction analyses were performed with a Smartlab 9KW diffractometer in high-pressure laboratory, Southern University of Science and Technology. The XRD patterns were collected using Cu kα_1 and kα_2 radiation in the range $2\theta = 10$–$90°$ with a step size of 0.02° and a counting time of 10 s per step.

Scanning electron microscope imaging was obtained using Zeiss Ultra 55 Field emission gun scanning electron microscope at Second Institute of Oceanography, State

Table 1 Experimental conditions

Sample no	Starting material	Grain sizes (μm)	W/R ratios	Time (days)	Product amount (%) from FTIR			
					Serpentine	talc	olivine	pyroxene
400 °C, 3.0 kbar								
HR69	Prt	< 30	0.76	20	99 (2.2)[a]	–	2 (1.7)	0
HR79	Prt	100–177	0.86	27	24 (3.4)	–	35 (1.4)	36 (2.0)
HR85	Prt	< 30	0.95	9	7 (5.0)	–	42 (2.1)	35
HR90	Prt	100–177	0.93	24	24 (3.6)	–	35 (1.5)	35 (0.2)
HR98	Prt	42–59	0.96	31	18 (3.1)	–	37 (1.3)	35
HR102	Prt	42–59	1.0	38	48 (3.4)	–	24 (1.4)	35 (1.0)
HR68	Spl-free prt	< 30	0.71	20	53 (3.5)	–	22 (1.5)	19 (2.0)
HR57	Ol	42–59	1.3	19	0.5	–	100	0.0
500 °C, 3.0 kbar								
HR19	Prt	82–106	1.3	19	3 (0.5)	7 (1.1)	59 (1.0)	32 (0.5)
HR21	Prt	82–106	0.90	30	4 (0.2)	9 (0.5)	57 (0.4)	31 (0.2)
HR71	Prt	< 30	0.97	20	6 (0.1)	13 (0.3)	53 (0.2)	28 (0.1)
HR82	Prt	< 30	1.0	36	6 (0.1)	14 (0.3)	53 (0.3)	28 (0.1)
HR81	Prt	100–177	1.0	21	7 (0.1)	3 (0.2)	59 (0.2)	32 (0.1)
HR70	Spl-free prt	< 30	0.97	20	5 (0.1)	11 (0.3)	55 (0.3)	29 (0.2)
HR83	Spl-free prt	< 30	1.0	36	5 (0.3)	11 (0.7)	55 (0.6)	30 (0.3)
HR46	Ol	100–177	1.5	18	0.5	0.0	100	0.0
500 °C, 8.0 kbar								
HR23	Prt	100–177	0.83	20	2.6 (0.8)	5.8 (1.7)	60 (1.6)	35 (1.6)
Fe24	Prt	100–177	0.50	20	2.5	6.2	59	35
500 °C, 20 kbar								
HR32	Prt	82–106	0.25	23	61 (1.5)	–	19 (0.6)	15 (0.9)
HR89	Prt	< 30	0.32	15	32 (1.2)	–	31 (0.5)	32 (0.7)
HR96	Prt	< 30	0.31	17	70 (3.5)	–	16 (1.4)	10 (2.0)
HR100	Prt	< 30	0.33	19	96 (3.6)	–	3 (2.9)	0
HR104	Prt	42–59	0.21	20	80 (1.5)	–	11 (0.6)	4 (0.9)
HR107	Prt	42–59	0.40	10	22 (5.3)	–	36 (2.2)	35 (0.3)

Prt peridotite, *Ol* olivine, *Spl-free prt* spinel-free peridotite

[a]Numbers in brackets represent standard deviation of analyses after at least three times ($\pm 1\delta$)

Oceanic Administration of China with an accelerating voltage of 5 kV.

Fourier transform infrared spectroscopy analyses were performed using a Bruker Vector 33 FTIR spectrometer at the Analytical and Testing Center of South China University of Technology. The spectra were obtained at wavenumbers ranging from 400 to 4000 cm^{-1} at a resolution of 4 cm^{-1}, and 32 scans were accumulated for each spectrum. KBr pellets were prepared by mixing approximately 1 mg of sample powder with 200 mg of KBr.

Raman measurements were performed with a LabRAM Aramis Raman spectrometer using a laser light at 523 cm^{-1} with a beam size of ~ 1 μm on the sample at Analytical and Testing Center of South China University of Technology. The spectra were recorded between 200 and 4000 cm^{-1}.

Chemical compositions of solid products were measured by a JOEL JXA 8100 electron microprobe at the Second Institute of Oceanography, State Oceanic Administration of China. Operating conditions of the electron beam were accelerating potential of 15 kV and beam current of 20 nA. A beam diameter of 15 μm was used for serpentine minerals to avoid devolatilization, and a beam diameter of 5 μm was used for olivine and pyroxene minerals. Calibration standards were jadeite (Si, Na), olivine (Mg), almandine garnet (Fe, Al), diopside (Ca), sanidine (K), chromium oxide (Cr), rutile (Ti), nickel silicide (Ni), rhodonite (Mn), and tugtupite (Cl). For Ni, Co, Mn, Cr and Cl, the counting time was 30 s for peak and 10 s for background; whereas, other elements were analyzed with 10 s for peak and 5 s for background.

Experimental results and discussion

Identification of secondary minerals

X-ray diffraction analyses of the experimental products show that olivine and pyroxene minerals were replaced by serpentine minerals for all the experiments of this study except those at 500 °C and 3.0–8.0 kbar, where serpentine and talc were produced (Fig. 1). The formation of serpentine was testified by typical infrared bands at 979 cm^{-1}, 1087 cm^{-1} and 3686 cm^{-1} (e.g., Fuchs et al. 1998; Lafay et al. 2014) (Fig. 2), where the bands at 979 cm^{-1} and 1087 cm^{-1} represent the Si–O group of serpentine and the band at 3686 cm^{-1} corresponds to the –OH group (e.g., Fuchs et al. 1998; Lafay et al. 2014). Talc has a typical stretching mode at 671 cm^{-1} for the Si–O–Mg group and stretching vibration at 3677 cm^{-1} for the –OH group (e.g., Liu et al. 2014). Scanning electron imaging suggests that the shape of serpentine minerals is characteristic of lizardite (Supporting information Figure S1). The Raman spectra of the experimental products at 500 °C showed intense peaks at 388 cm^{-1} and 3693 cm^{-1}, and at 381 cm^{-1} and 3686 cm^{-1}, for experiments at 3.0 and 20 kbar,

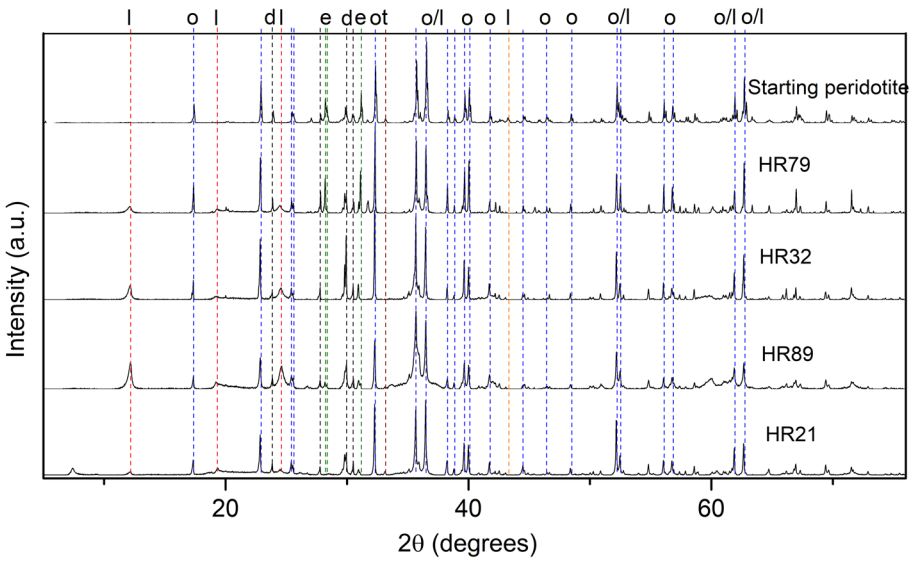

Fig. 1 XRD patterns of the experimental products of this study. *o* olivine, *l* lizardite, *e* enstatite, *d* diopside, *t* talc

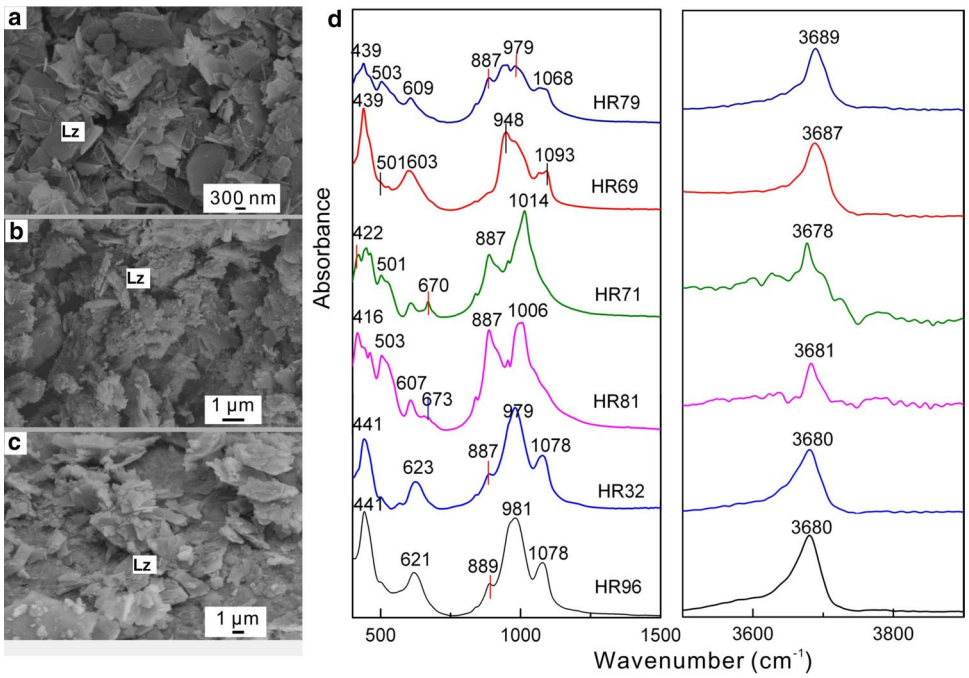

Fig. 2 Identification of the experimental products using scanning electron microscopy imaging and Fourier transform infrared spectroscopy analyses. **a** HR79, 400 °C and 3.0 kbar, **b** HR81, 500 °C and 3.0 kbar, and **c** HR32, 500 °C and 20 kbar. **d** FTIR spectra of the experimental products

respectively (Figure S1). These Raman peaks correspond to those of lizardite (Auzende et al. 2004), and the shift of peak positions at lower wavenumbers with increasing pressure has been reported by Auzende et al (2004). Antigorite, however, was not observed in all the experimental products of this study.

Despite occurrences of brucite in many previous experiments (e.g., Malvoisin et al. 2012; McCollom et al. 2016), it was absent in the experimental products of this study. This may be attributed to multiple factors: (1) relatively high temperatures. Thermodynamic models suggest that the production of brucite during serpentinization decreases greatly with increasing temperatures, and brucite may be absent at temperatures of higher than 350 °C (McCollom and Bach 2009). (2) Silica activity. Compared to olivine, peridotite has silica activity around 1–2 orders of magnitude higher (Allen and Seyfried 2003). As suggested by thermodynamic models, the stability of brucite decreases greatly at higher silica activity, under which conditions brucite reacts with silica [Reaction (1)], leading to the production of serpentine minerals (Frost and Beard 2007):

$$\underset{\text{olivine}}{Mg_2SiO_4} + 4\underset{\text{brucite}}{Mg(OH)_2} + 3\underset{\text{silica}}{SiO_2} = 2\underset{\text{serpentine}}{Mg_3Si_2O_5(OH)_4}. \quad (1)$$

Consistently, previous experiments have shown that brucite is formed after the serpentinization of olivine (e.g., Lafay et al. 2012; Malvoisin et al. 2012), and it is absent after peridotite serpentinization (e.g., Marcaillou et al. 2011; Huang et al. 2017a, b).

Quantification of serpentinization kinetics

The extent of reaction, which is defined as the proportions of serpentine and (±) talc in the experimental products, was quantified by Fourier transform infrared spectroscopy (Table 1). This technique is very sensitive to the presence of serpentine minerals, which can detect < 0.1 wt% of serpentine (Foresti et al. 2003). Infrared spectroscopy has been used to determine the proportions of serpentine in soil samples and experimental products after serpentinization by calibrating the integrated areas of the –OH band of serpentine (e.g., Foresti et al. 2003; Lafay et al. 2012, 2014; Huang et al. 2017a). For peridotite experiments with serpentine as the major secondary mineral, the standard curve for calibration was established by preparing mechanical mixtures of serpentine and peridotite with the proportions of serpentine ranging from 10% to 90%. The standard curve has been illustrated in Fig. 3a, showing that the percentage of serpentine has a positive correlation with $\log(A_{3698}/A_{503})$ ($R^2 = 0.98$), where A_{3698} is the integrated intensity of –OH group in serpentine, and A_{503} is the integrated intensity of Si–O group in olivine. For peridotite experiments with serpentine and talc as the main secondary minerals, the standard curve for calibration was established based on the infrared spectra of mechanical mixtures of peridotite, serpentine and talc. As shown in Fig. 3b, the percentage of serpentine and talc in the mechanical mixtures is positively correlated with integrated intensity ratios $(A_{609} + A_{670})/A_{503}$ ($R^2 = 0.97$, Fig. 3b), where A_{609} is the integrated intensity of Mg–O band in serpentine, A_{670} is the integrated intensity of Si–O–Mg band in talc, and A_{503} is the integrated intensity of Si–O band in olivine. Repeated analyses (> three times) showed that the precision of calibration was ±4%.

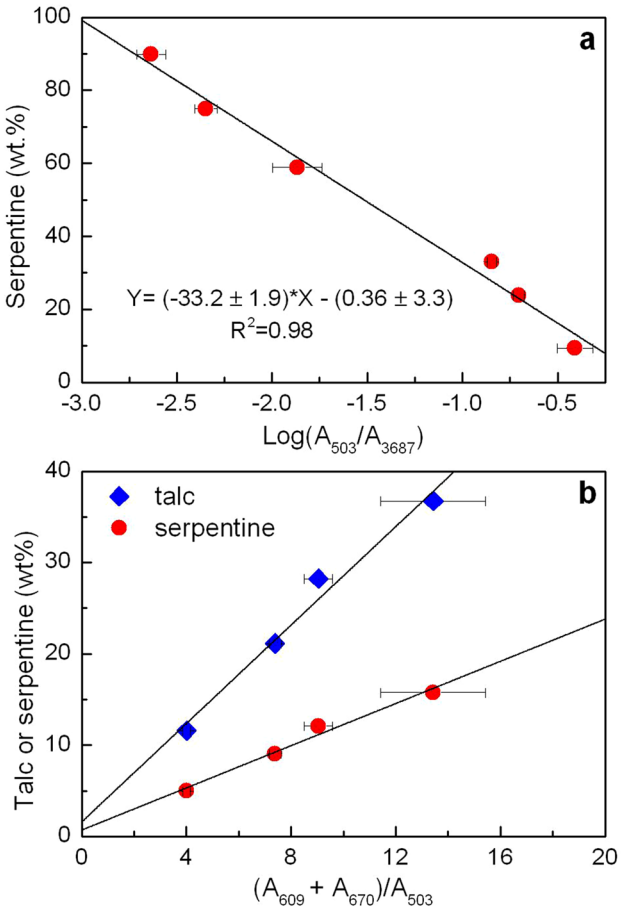

Fig. 3 Standard curves used to calibrate the reaction extent. The curve in **a** was used to obtain reaction progresses in experiments at 400 °C and 3.0 kbar and at 500 °C and 20 kbar with serpentine as the main secondary minerals, and the curves in **b** were used to obtain reaction progresses in experiments at 500 °C and 3.0–8.0 kbar with serpentine and talc as major secondary minerals. The proportion of serpentine was calibrated according to $Y = (1.2 \pm 0.1) \times X + (0.7 \pm 1.1)$ ($R^2 = 0.97$), and the percentage of talc was calculated based on $Y = (2.7 \pm 0.3) \times X + (1.7 \pm 2.5)$ ($R^2 = 0.97$)

In olivine experiments at 400–500 °C and 3.0 kbar, < 1% of reaction extent was achieved after around 18 days (Table 1), which agrees well with the previous experimental studies (e.g., Allen and Seyfried 2003; Malvoisin et al. 2012; McCollom et al. 2016). In contrast, for experiments

at 400–500 °C and 3.0 kbar with peridotite as the starting reactant, the extent of reaction was significantly enhanced, e.g., for those at 400 °C and 3.0 kbar with starting grain sizes of 42–59 μm, 18% of reaction extent was achieved within 31 days, which increased to 48% after longer time (48 days). The kinetics of peridotite serpentinization at 400 °C and 3.0 kbar and at 500 °C and 20 kbar displayed a sigmoidal kinetic behavior, with an initially slow reaction rate and a more rapid reaction rate after longer experimental duration (Fig. 4). The serpentinization kinetics were successfully fitted with an empirical Eq. (2):

$$\xi = \xi_{\max} / \left(1 + \exp\left(-\frac{t - t_{1/2}}{b}\right)\right), \quad (2)$$

where $\xi_{\max}$ is the maximum reaction extent (%) achieved during serpentinization, ξ is the reaction extent (%) at any time t (day), $t_{1/2}$ is the duration when half of the maximum of reaction extent was reached, and b is a constant. The initial rate of serpentinization, ν_0 (1/day), was calculated by the following expression:

$$\nu_0 = \frac{\xi_{\max}}{100 \times t_{1/2}}. \quad (3)$$

A sigmoidal regression by the least-squares method was performed to obtain the kinetic parameter $t_{1/2}$, and subsequently, the initial rate of serpentinization was calculated (Table 2). The initial rate of serpentinization was found to be inversely proportional to the geometrical surface area of the starting peridotite grains. For experiments at 400 °C and 3.0 kbar with starting grain sizes of < 30 μm, the initial rate of serpentinization was 8.93×10^{-7} s^{-1}, and it slightly decreased to 2.89×10^{-7} s^{-1} for starting grain sizes of 100–177 μm. This suggests that fluid/peridotite interface depending on starting grain sizes of peridotite greatly influences the initial rate of serpentinization.

The kinetic data of this study were also fitted with the Avrami equation (Avrami 1939), which is expressed as:

$$\xi = 1 - \exp(-kt^n), \quad (4)$$

where k is a rate constant and n is an Avrami exponent. Converting Eq. (4) into logarithms:

$$\ln(-\ln(1 - \xi)) = \ln k + n \ln t. \quad (5)$$

The rate constant (k) and Avrami exponent (n) were obtained by fitting ln(−ln(1 − ξ)) versus lnt (Fig. 5). The Avrami exponent was > 1 for experiments at 400 °C and 3.0 kbar and at 500 °C and 20 kbar (Fig. 5), which indicates that the serpentinization reactions may be interface controlled. The rate constant k is expressed as $G \times S$, where G (m s^{-1}) is defined as the reaction rates and S is the specific

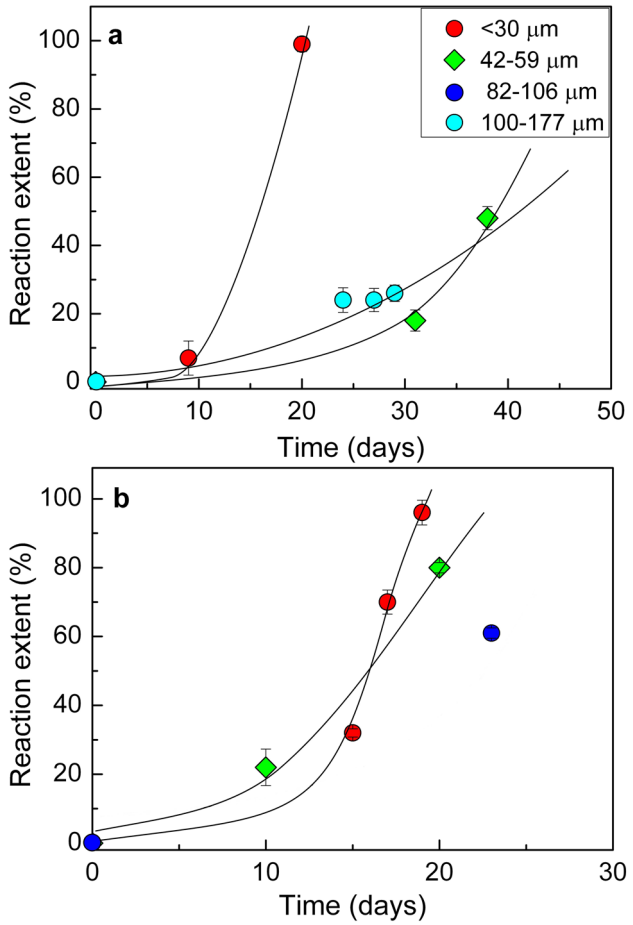

Fig. 4 Serpentinization degree (%) as a function of time (days) for experiments at **a** 400 °C and 3.0 kbar, and **b** 500 °C and 20 kbar. Data were fitted by a sigmoidal kinetic model

Table 2 Kinetic parameters obtained from the sigmoidal model

T (°C)	P (kbar)	Starting grain size (μm)	$\xi_{\max}$		$t_{1/2}$ (days)	Initial rate (1/s)	Fitting r^2
			Exp.	calc			
400	3.0	< 30	99	100	12.96 ± 0.01	8.93E-7 ± 6.89E-10	0.999
400	3.0	42–59	38	100	38.39 ± 0.01	3.01E-7 ± 7.80E-11	0.999
400	3.0	100–177	26	100	40.10 ± 5.86	2.89E-7 ± 4.90E-8	0.906
500	20	< 30	96	100	15.92 ± 0.09	7.27E-7 ± 4.13E-9	0.997
500	20	42–59	80	100	14.79 ± 0.30	7.82E-7 ± 1.62E-8	0.998

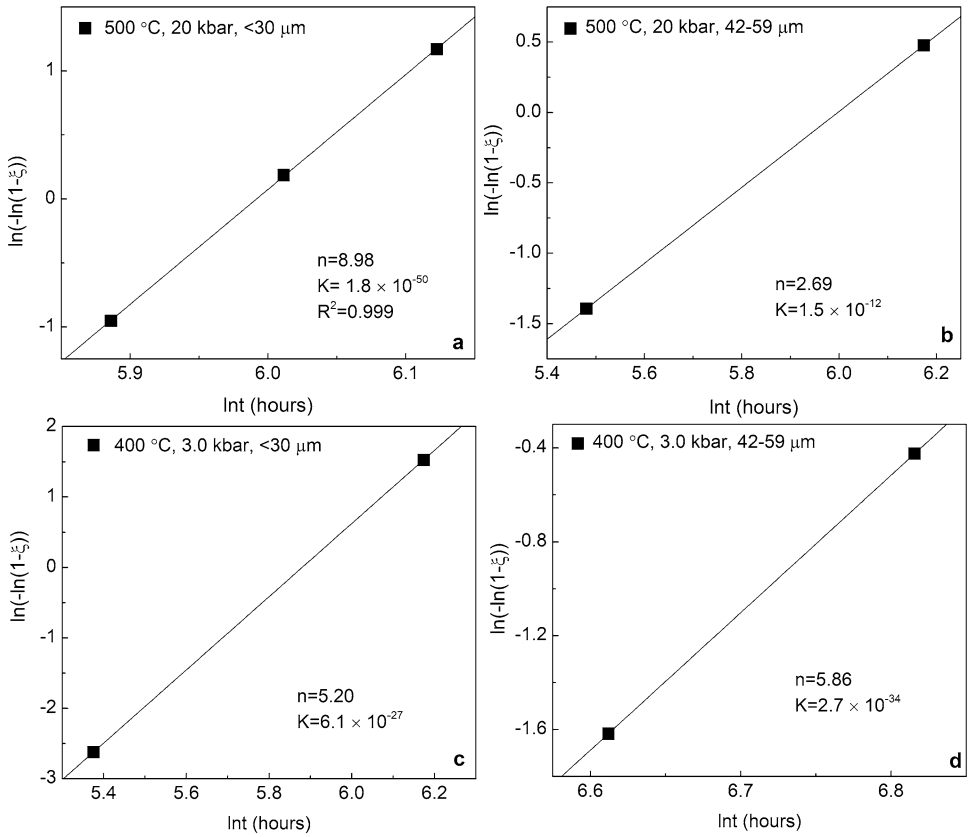

Fig. 5 The fit of serpentinization kinetics of this study with Avrami equation. **a** 500 °C and 20 kbar with starting grains of peridotite < 30 μm; **b** 500 °C and 20 kbar with starting grains of peridotite 42–59 μm; **c** 400 °C and 3.0 kbar with starting grains of peridotite < 30 μm; and **d** 400 °C and 3.0 kbar with starting grains of peridotite 42–59 μm

surface area (Supporting information Table S1). For experiments at 400 °C and 3.0 kbar, the reaction rates were calculated to be 2.68×10^{-34} m s^{-1} for starting grain sizes of 42–59 μm, which increased to 6.15×10^{-27} m s^{-1} for starting grain sizes of < 30 μm. In contrast, for experiments at 500 °C and 20 kbar, the reaction rates were 1.48×10^{-12} m s^{-1} for starting grains sizes of 42–59 μm, which became even slower for starting grain sizes of < 30 μm, 1.79×10^{-50} m s^{-1}, possibly reflecting that the serpentinization reactions at high pressures may not be solely controlled by dissolution of olivine and pyroxene minerals.

Influence of pressures, pyroxene, and spinel on serpentinization rates

Previous experiments conducted at ≤ 300 °C and 500 bars have revealed that the serpentinization of olivine invokes coupled dissolution and precipitation processes, and the dissolution of olivine may be a controlling factor during serpentinization (e.g., Lafay et al. 2012, 2014; Malvoisin et al. 2012). Consistently, dissolution features were produced after the serpentinization of peridotite for experiments of this study (Fig. 5). The ultra-slow rates at the early stage of serpentinization (~ 10 days), however, suggest that serpentinization at 400 °C and 3.0 kbar and at 500 °C and 20 kbar may be rate limited by the nucleation and growth of lizardite rather than the dissolution of olivine and pyroxene minerals, due to positive temperature dependence of the dissolution of olivine and pyroxene minerals (Wood and Walther 1983). The difficulty in nucleating lizardite at the early stage of serpentinization may be closely associated with a positive Gibbs energy of forsterite hydrothermal alteration (ΔG_{rxn}) at temperatures of ≥ 350 °C [Eq. (6)]:

$$\underset{\text{Forsterite}}{2Mg_2SiO_4} + 3H_2O = \underset{\text{Brucite}}{Mg(OH)_2} + \underset{\text{Serpentine}}{Mg_3Si_2O_5(OH)_4}. \quad (6)$$

This is supported by very low extent of reaction achieved in olivine-experiments at 400–500 °C and 3.0 kbar, which agrees well with the previous experimental studies (e.g., Malvoisin et al. 2012; McCollom et al. 2016). However, the kinetics of peridotite serpentinization under the same T–P conditions were significantly enhanced. In particular, several lines of evidence suggest that olivine was replaced by serpentine minerals with the presence of pyroxene and spinel: First, backscattered electron imaging of the experimental products directly shows that olivine was replaced by serpentine minerals (Fig. 6). Moreover, a decrease in the intensities of X-ray peaks for olivine was associated with an increase in the intensities of X-ray peaks for serpentine and (±) talc (Fig. 1). Additionally, the percentage of residual olivine in the experimental products was ranged from 2% to 42% (Table 1), which is much lower than the proportion of

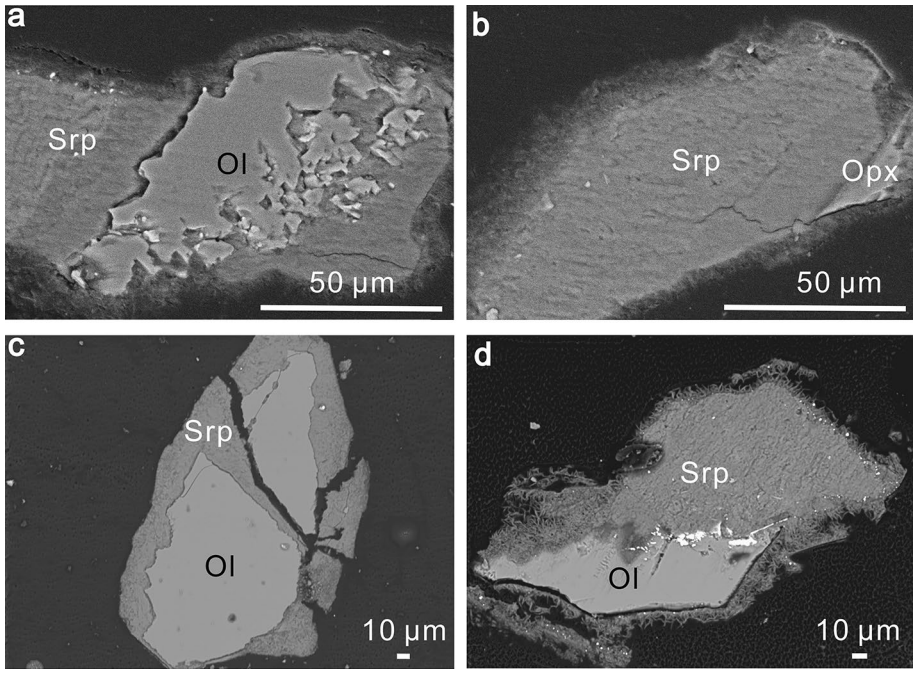

Fig. 6 Backscattered electron images of the reaction products. **a** HR78, 400 °C and 3.0 kbar, and **b** HR32, 500 °C and 20 kbar. **a**, **b** show the replacement of olivine by serpentine minerals, leading to the formation of dissolution patterns. **c** HR21, 500 °C and 3.0 kbar, olivine was transformed into serpentine minerals. **d** HR21, olivine was replaced by talc and iron oxide

olivine in primary peridotite (~65%). All these indicate that olivine can be transformed into serpentine minerals under the investigated conditions.

The replacement of olivine by serpentine minerals in the experiments of this study suggests that Gibbs energy of forsterite hydrothermal alteration (ΔG_{rxn}) is negative. In contrast, Allen and Seyfried (2003) performed experiments at 400 °C and 500 bars with mixtures of olivine and orthopyroxene as starting reactants, and they found that olivine adjacent to orthopyroxene still remained fresh after 70 days of reaction. This is mainly attributed to a positive ΔG_{rxn} for forsterite hydrolysis at 400 °C and 500 bars (Allen and Seyfried 2003). However, Nakatani and Nakamura (2016) showed that the serpentinization of olivine can proceed at 400 °C and 13 kbar, forming serpentine and brucite. This implies that pressure may enhance the rates of serpentinization, which is further supported by an increase in the rates of serpentinization in experiments of this study at 500 °C. For experiments at 500 °C and 3.0 kbar using peridotite with starting grain sizes of < 30 μm, 19% of reaction progress was achieved after 20 days; for experiments at 500 °C and 20 kbar using peridotite with starting grain sizes of < 30 μm, 96% of reaction extent was achieved after 19 days (Table 1).

The increase in the rates of serpentinization at higher pressures may be associated with a decrease in Gibbs energy of forsterite hydrolysis [Reaction (4)]. Such hypothesis was testified by performing thermodynamic calculations using customized thermodynamic database compiled with SUPCRT92 (Johnson et al. 1992). The calibration has revealed that ΔG_{rxn} for forsterite hydrolysis at 400 °C and 500 bars is 7.89 kcal/mol, which agrees well with Allen and Seyfried (2003). Gibbs energy of forsterite hydrothermal alteration as a function of pressure has been illustrated in Fig. 7, showing that ΔG_{rxn} decreases greatly with increasing pressures. Despite such decrease, ΔG_{rxn} of forsterite hydrolysis at 400–500 °C and 3.0 kbar is still positive, which cannot account for the observed hydrothermal alteration of olivine under these conditions. This indicates that the serpentinization of olivine at temperatures of ≥ 350 °C may not be solely influenced by pressures, but also affected by the presence of pyroxene and spinel.

Electron microprobe analyses of the experimental products in this study suggest that serpentine formed after the hydrothermal alteration of pyroxene contained much less SiO_2 than that of primary pyroxene (Figs. 8, S2; Table S2). In contrast, serpentine formed after the hydrothermal alteration of olivine had more SiO_2 than that of primary olivine (Figs. 8, S1). As suggested by experimental simulations, hydrothermal alteration of pyroxene released dissolved SiO_2 around one order of magnitude higher than that leached after hydrothermal alteration of olivine (e.g., Allen and Seyfried 2003). This indicates that the SiO_2 released from pyroxene minerals was involved into olivine hydrolysis:

$$\underset{\text{Forsterite}}{3Mg_2SiO_4} + \underset{\text{Silica}}{SiO_{2(aq)}} + 4H_2O = \underset{\text{Serpentine}}{2Mg_3Si_2O_5(OH)_4}. \quad (7)$$

The role of silica on the hydrothermal alteration of olivine was examined by calibrating ΔG_{rxn} of forsterite hydrolysis [Reaction (5)]. As illustrated in Fig. 7b, the involvement of silica during serpentinization results in a negative ΔG_{rxn} of forsterite hydrolysis at 400–500 °C and 3.0 kbar (Fig. 7b),

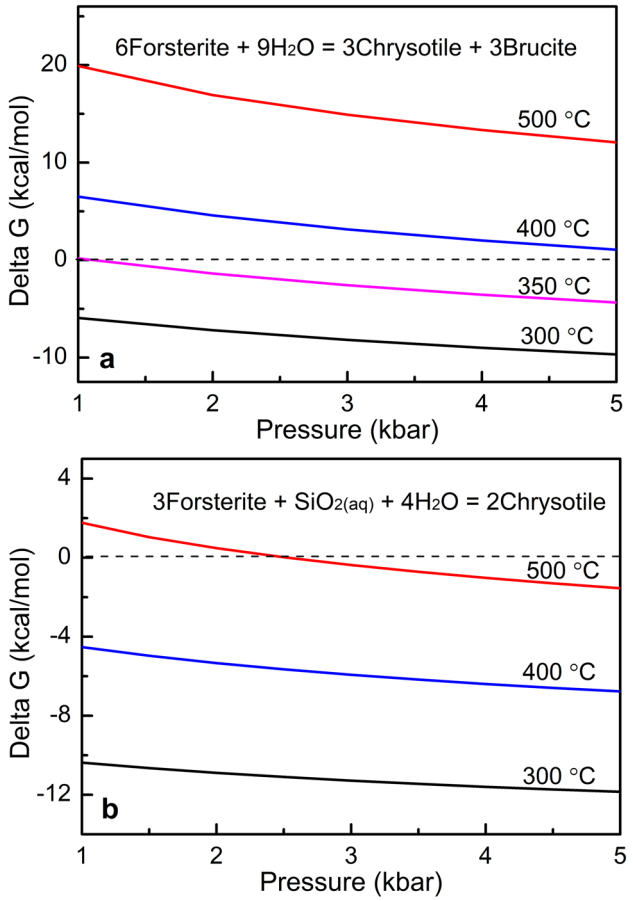

Fig. 7 Effect of pressure on Gibbs energy of olivine hydrolysis at temperatures of 300–500 °C. **a** Olivine hydrolysis via 6Forsterite + $9H_2O$ = 3Chrysotile + 3Brucite, and **b** olivine hydrolysis via 3Forsterite + $SiO_{2(aq)}$ + $4H_2O$ = 2Chrysotile. With the involvement of silica, Gibbs energy of olivine hydrolysis becomes more negative at higher pressures

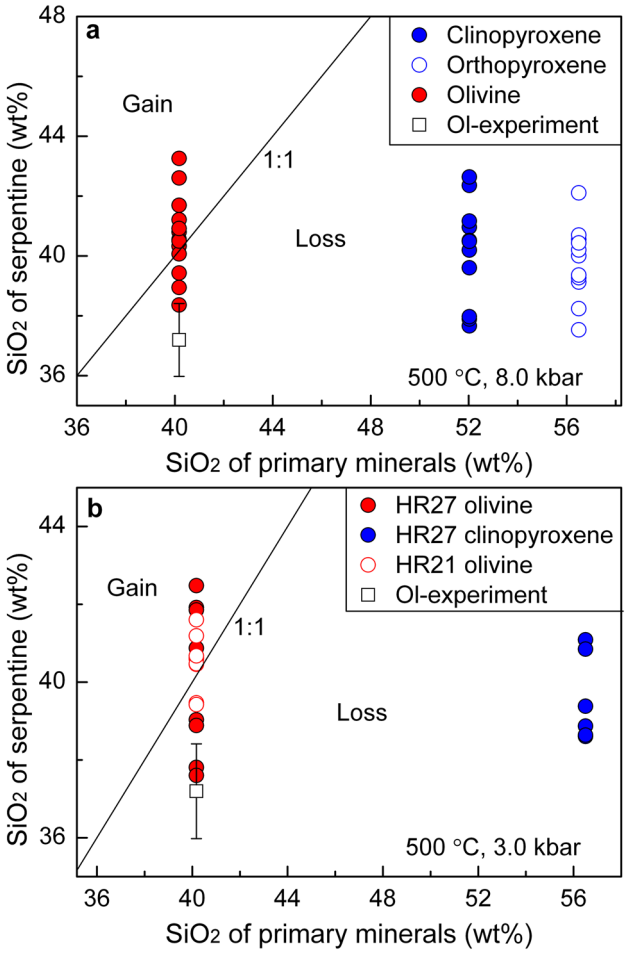

Fig. 8 Partitioning of SiO_2 between primary minerals (olivine, orthopyroxene and clinopyroxene) and their coexisting serpentine in experiments **a** at 500 °C and 8.0 kbar and **b** at 500 °C and 3.0 kbar. "Ol-experiment" represents experiments performed at 311 °C and 3.0 kbar with olivine as the starting material (Huang et al. 2017a). The data above the 1:1 line indicate a gain of SiO_2 during serpentinization, and the data below the 1:1 line suggest a loss of SiO_2. *Ol* olivine, *opx* orthopyroxene, *cpx* clinopyroxene

which accounts well for the observed rates of behavior in the experiments of this study. Consistently, Martin and Fyfe (1970) showed that 5% of reaction extent was achieved in experiments at 350 °C and 2.2 kbar using solely forsterite, and 20% of reaction extent was reached for experiments with mixtures of forsterite and enstatite as starting materials. Moreover, thermodynamic models suggest that for experiments with harzburgite at 350 °C and 350 bars, 35–55% of the original olivine is converted into serpentine minerals before reaching equilibrium (McCollom and Bach 2009). All these indicate that pyroxene minerals may promote the hydrothermal alteration of olivine.

The role of pyroxene minerals on the kinetics of serpentinization was studied, and hydrothermal experiments were performed at 400–500 °C and 3.0–20 kbar with mechanical mixtures of pyroxene and olivine (i.e., spinel-free peridotite). Compared to olivine-only experiments, an increase in the rates of serpentinization was observed (Fig. 9), e.g., in experiments at 400 °C and 3.0 kbar with mechanical mixtures of pyroxene and olivine, 53% of reaction extent was reached for starting grain sizes of < 30 μm after 20 days, which is much higher than the extent of reaction achieved in olivine-only experiments (< 1%). This suggests that pyroxene accelerates the hydrothermal alteration of olivine.

The experimental results of this study indicate that the serpentinization of individual minerals (e.g., olivine and pyroxene minerals) differs greatly from the hydrothermal alteration of their combinations (peridotite). To illustrate the serpentinization of olivine and pyroxene minerals during the hydrothermal alteration of peridotite, we quantified the proportions of serpentinized olivine (pyroxene), which are the mass ratios between olivine (pyroxene) that was transformed into serpentine and primary olivine (pyroxene),

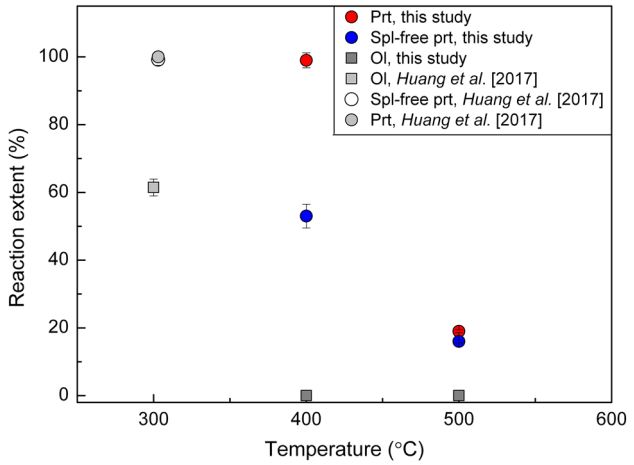

Fig. 9 Influence of pyroxene and spinel on serpentinization kinetics. Experiments at 400 °C and 3.0 kbar and at 500 °C and 3.0 kbar were conducted with run duration of 20 days. In experiments at 400 °C and 3.0 kbar, spinel and pyroxene greatly increase the rates of olivine serpentinization, consistent with Huang et al (2017a). At 500 °C and 3.0 kbar, the influence of spinel on the serpentinization of olivine is negligible, and pyroxene greatly increases the kinetics of olivine serpentinization

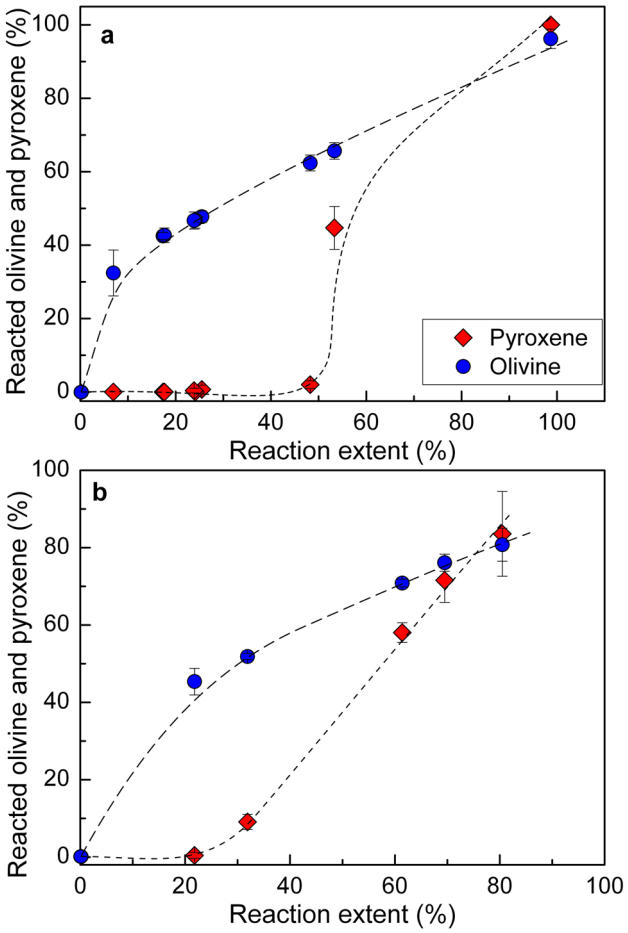

Fig. 10 The proportions of reacted olivine and pyroxene (%) as a function of reaction extent (%). **a** 400 °C and 3.0 kbar, and **b** 500 °C and 20 kbar

$X = m_{react}/m_{primary}$. The procedures for calibrating the percentage of serpentinized olivine and pyroxene have been detailed in previous experimental studies (Huang et al. 2017a, 2019). As illustrated in Fig. 10, the proportions of serpentinized pyroxene were close to zero at the early stage of serpentinization (e.g., reaction extent of $<20\%$). With progressive serpentinization, the proportions of serpentinized pyroxene increased, while they were still much lower than the proportions of serpentinized olivine at reaction extent of $<80\%$. This indicates that pyroxene minerals were serpentinized at much slower rates compared to olivine during peridotite serpentinization. In contrast, previous experiments using individual olivine and pyroxene minerals have shown that pyroxene minerals were serpentinized at much faster rates than olivine at temperatures of ≥ 350 °C (Martin and Fyfe 1970). This indicates that the serpentinization of pyroxene minerals was impeded during the hydrothermal alteration of peridotite. This is possibly associated with transport of silica released from pyroxene minerals to the serpentinization of olivine. Silica triggers the hydrothermal alteration of olivine, and consequently the serpentinization of pyroxene minerals may be retarded. The largely scattered SiO_2 contents of serpentine minerals formed after olivine hydrothermal alteration indicate that silica may be locally transported (Table S2). This indicates that serpentinization at temperatures of 400–500 °C may be limited by transportation of SiO_2 especially at the start of experiment, which may explain the ultra-slow rates at the early 10 days.

On the other hand, the kinetics of olivine serpentinization can be greatly influenced by spinel. The effect of spinel was investigated by performing hydrothermal experiments at 400–500 °C and 3.0 kbar with spinel-bearing and spinel-free peridotite (Table 1). For experiments at 400 °C and 3.0 kbar, the extent of reaction after serpentinization of spinel-bearing peridotite was significantly higher than that after hydrothermal alteration of spinel-free peridotite within the same experimental duration, suggesting that spinel greatly enhances the serpentinization of olivine. However, for experiments at 500 °C and 3.0 kbar, the extent of reaction reached during the serpentinization of spinel-bearing peridotite was essentially the same as that achieved after the hydrothermal alteration of spinel-free peridotite (Fig. 9), suggesting that the influence of spinel on the kinetics of serpentinization is minor. Hydrothermal experiments with mechanical mixtures of olivine and spinel were also performed at 500 °C and 3.0 kbar, and olivine was essentially non-altered after around 20 days. This suggests that silica released from pyroxene is a requisite for the serpentinization of olivine at temperatures of ≥ 350 °C, which greatly decreased the Gibbs free energy of the serpentinization of olivine. Spinel, however, may

kinetically influence the serpentinization of olivine rather than thermodynamically.

Our recent experimental study shows that pyroxene and spinel greatly accelerate the hydrothermal alteration of olivine, resulting from releases of aluminum from pyroxene and spinel (Huang et al. 2017a). Aluminum accelerates the hydrothermal alteration of olivine by around 1–2 orders of magnitude (Andreani et al. 2013). To study the mobility of aluminum in experiments of this study, we determined chemical compositions of olivine- and pyroxene-derived serpentine minerals using electron microprobe. It shows that pyroxene-derived serpentine has much less Al_2O_3 compared to that of primary pyroxene (Figure S3), e.g., for experiments at 400 °C and 3.0 kbar on peridotite, serpentine formed after orthopyroxene serpentinization has 3.43 ± 1.03 wt% Al_2O_3, much less than the Al_2O_3 contents of primary orthopyroxene (4.1 ± 0.20 wt%). Therefore, pyroxene minerals released some of their Al during peridotite serpentinization. In contrast, serpentine formed after olivine serpentinization has much larger Al_2O_3 contents compared to the Al_2O_3 contents of primary olivine. This indicates that aluminum released from pyroxene minerals was involved in the serpentinization of olivine, which agrees well with the previous results (e.g., Dungan 1979; Golightly and Arancibia 1979; Hébert et al. 1990; Huang et al. 2017a). Releases of aluminum from spinel were indicated by the formation of magnetite rind around primary spinel in experiments at 400–500 °C and 3.0 kbar; while, Al-depleted ferrichromite and (±) magnetite rinds were produced at 500 °C and 20 kbar (Figure S4). The role of aluminum on the serpentinization processes, however, is minor especially at 500 °C and 3.0 kbar, indicated by very low reaction extent (< 10%) in experiments with mechanical mixtures of olivine and Al_2O_3 fine powders as starting reactants.

Comparisons with previous studies

Previous experiments on the kinetics of serpentinization were performed mostly at temperatures of ≤ 300 °C and 500 bars with olivine as the starting reactant (e.g., Martin and Fyfe 1970; Wegner and Ernst 1983; Malvoisin et al. 2012; Lafay et al. 2012, 2014; McCollom et al. 2016). The kinetics of olivine serpentinization as a function of temperature display a bell-shaped curve with a maximum centered around 270 °C for synthetic forsterite and ~ 300 °C for natural olivine, and they decreased by around 1–2 orders of magnitude at temperatures of higher than 350 °C (Martin and Fyfe 1970; Wegner and Ernst 1983; Malvoisin et al. 2012; McCollom et al. 2016). In contrast, the experiments of this study show that the kinetics of peridotite serpentinization at 400 °C and 3.0 kbar and at 500 °C and 20 kbar are around 1–3 orders of magnitude faster than the rates of olivine serpentinization under the same T–P conditions. Temperature

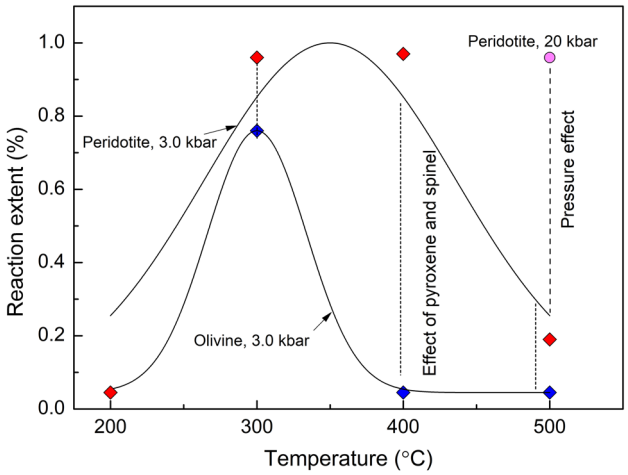

Fig. 11 Reaction extent (%) as a function of temperature. Data at 200–300 °C and 3.0 kbar are from Huang et al. (2017a) and others are from the experiments of this study

dependence of the rates of peridotite serpentinization has been illustrated in Fig. 11. It shows that pressure greatly influences the rates of serpentinization, e.g., the kinetics of peridotite serpentinization at 500 °C and 3.0–8.0 kbar are around four times slower than the rates of reaction at 500 °C and 20 kbar (Table 1). Consistently, Nakatani and Nakamura (2016) have studied the kinetics of serpentinization at 400–580 °C and 13–18 kbar, and they showed that olivine was transformed into serpentine at 400 °C and 13 kbar. The rates of olivine serpentinization in Nakatani and Nakamura (2016) were much faster compared to those at low pressures (e.g., 500 bars) (e.g., Allen and Seyfried 2003), indicating that pressure promotes the serpentinization of olivine.

The influence of pressure on the rates of serpentinization at 500 °C may be associated with mineral assemblages of run products. For experiments at 500 °C and 3.0–8.0 kbar with peridotite as the starting reactant, olivine was transformed into serpentine, and pyroxene minerals were replaced by serpentine and talc; for experiments at 500 °C and 20 kbar, serpentine minerals were the major secondary minerals without the formation of talc. Electron microprobe analyses of the run products show that talc has ~ 60 wt% SiO_2, much larger than the SiO_2 contents of serpentine (Table S2). Therefore, the formation of talc at 500 °C and 3.0 kbar suggests higher silica activity compared to high-pressure experiments. Despite the relatively low silica activity of our experiments at 500 °C and 20 kbar, pressure may not be the controlling factor for silica activity. Nakatani and Nakamura (2016) performed experiments at 500 °C and 18 kbar with mixtures of olivine and orthopyroxene as starting reactants, and the major secondary minerals were composed of talc and serpentine. This indicates that mineralogy of starting reactants (e.g., the presence of spinel) may greatly influence the

formation of talc and silica activity. Spinel in experiments of this study at 500 °C and 3.0 kbar was surrounded by a thin layer of magnetite. In contrast, spinel in experiments at 500 °C and 20 kbar was reacted with SiO_2-rich aqueous fluids, which was more extensively altered, producing ferrichromite and chlorite (Figure S3). This may induce releases of more aluminum from spinel at high pressures, and consequently the rates of reaction can be accelerated.

Compared to the kinetics of serpentinization reported by Nakatani and Nakamura (2016), the kinetics of this study are around 10–20 orders of magnitude slower. The discrepancy may be associated with multiple factors: (1) analytical method. Nakatani and Nakamura (2016) quantified the amount of serpentine and talc in the experimental products on the basis of the area fraction of relict minerals with respect to all minerals ($R = A_{relict}/A_{solid}$), with the assumption that the density of relict minerals (serpentine and talc) is quite comparable with that of primary olivine and pyroxene minerals. However, the serpentinization of olivine and pyroxene minerals typically forms a porous matrix (Nakatani and Nakamura, 2016). This suggests that serpentinization processes may be associated with volume changes, which may lead to an increase in the surface area and, consequently, faster rates of serpentinization can be obtained. (2) secondary minerals in the experimental products. Nakatani and Nakamura (2016) performed experiments mostly with mixtures of orthopyroxene and clinopyroxene, and mixtures of olivine and orthopyroxene, and the secondary minerals were serpentine and talc. In contrast, the main secondary minerals of this study were serpentine. Compared to serpentine (~40 wt%), talc has larger SiO_2 contents (~60 wt%). This indicates that silica activity (a_{SiO2}) in experiments of Nakatani and Nakamura (2016) may be higher than that of this study, which may consequently influence the serpentinization kinetics. (3) chemical compositions of starting fluids. Distilled water was used in the experiments of Nakatani and Nakamura (2016), and saline solutions (0.5 M NaCl) were taken in this study. As suggested by Lamadrid et al. (2017), the rates of olivine serpentinization are strongly controlled by fluid salinity, which decreased by 1-2 orders of magnitude with increasing fluid salinity from 1 wt% to 10 wt% NaCl. The influence of fluid salinity on serpentinization rates may be associated with the structual incorporation of chlorine into serpentine (Huang et al. 2018). (4) kinetic behavior. The kinetics of serpentinization in Nakatani and Nakamura (2016) described a fast mass transfer followed by a slow equilibration of mass transfer. In contrast, the kinetic data of this study displayed a sigmoidal behavior, with a sluggish rate at the early stage of serpentinization and followed by a faster rate with progressive hydrothermal reaction. All these factors may induce a great discrepancy between serpentinization kinetics reported in Nakatani and Nakamura (2016) and those of this study.

Geological implications

Serpentinites in subduction zones form under a wide range of temperatures and pressures, and they may have three possible protoliths: (1) forearc mantle peridotite is hydrated by aqueous fluids released from subducted slabs, (2) abyssal peridotites hydrated at shallow depths near the seafloor and mid-oceanic ridges and, (3) hydrated ultramafic cumulates (e.g., Saumur et al. 2010; Evans et al. 2013). Geophysical models have utilized the kinetics of serpentinization especially data from Martin and Fyfe (1970) to quantify the proportions of serpentine in subduction zones (e.g., Iyer et al. 2010, 2012). However, previous experiments about serpentinization kinetics were performed at relatively low temperatures (e.g., ≤300 °C) and low pressures (e.g., ≤3 kbar) mostly with olivine as the starting reactant (e.g., Malvoisin et al. 2012; Lafay et al. 2012, 2014; McCollom et al. 2016; Huang et al. 2017a), and they may not apply to serpentinization at high pressures associated with subduction zones where olivine is commonly associated with pyroxene and spinel.

The three common serpentine minerals are lizardite, chrysotile, and antigorite. As suggested by thermodynamic models, the stability temperature of lizardite is lowest (i.e., 125 °C), followed by chrysotile (180 °C), and the stability temperature of antigorite is highest (235 °C) (e.g., Evans et al. 1976). In particular, dehydration experiments show that antigorite can be stable at 700 °C and relatively high pressures (e.g., ~24 kbar) (Ulmer and Trommsdorff 1995). All these observations suggest that antigorite is the predominant serpentine mineral in subduction zones especially at great depths (e.g., O'Hanley 1996). Consistently, petrological observations of natural serpentinites from the Alpine paleo-accretionary wedge show that lizardite and chrysotile are the dominant serpentine minerals at temperatures below 300 °C, and antigorite is the main stable serpentine mineral at temperatures above 390 °C (e.g., Schwartz et al. 2013; Guillot et al. 2015). However, antigorite is always absent in hydrothermal experiments performed within the stability field of antigorite (Malvoisin et al. 2012; McCollom et al. 2016; Huang et al. 2017a, b), except one experiment of Nakatani and Nakamura (2016) conducted at 580 °C and 18 kbar with mechanical mixtures of olivine and orthopyroxene as starting reactants. Petrological observations also suggest that antigorite cannot form directly from olivine hydrolysis (Wicks and Whittaker 1977), while it can be produced after the metasomatism of lizardite by CO_2-bearing fluids (e.g., Wu et al. 2018). Therefore, lizardite may be a precursor of antigorite in subduction zones at great depths. The stability of lizardite can be greatly influenced by multiple factors, including the incorporation of Al and Fe, and pH and chemical compositions of starting fluids (e.g., Seyfried and Dibble 1980; O'Hanley et al. 1989; Hilairet et al. 2006;

Huang et al. 2017a, b). Aluminum enlarges the stability temperature range of lizardite, and lizardite can be stable at 400–500 °C (O'Hanley et al. 1989). Consistently, our experimental results have revealed that lizardite can be stable up to 500 °C and 20 kbar. Pressure (up to 10 GPa), however, has a minor influence on the stability field of serpentine minerals (Hilairet et al. 2006). On the other hand, Costa et al. (2008) proposed that antigorite may not result from high-temperature prograde metamorphism, and it may be produced at temperatures well below 300 °C. Therefore, the formation mechanisms of antigorite still remain poorly constrained, which may explain the discrepancy of experimental results from observations of natural samples. Despite such discrepancy, the experimental results of this study may still be applied to serpentinization of ultramafic rocks in natural geological settings where water is abundant.

Conclusions

The kinetics of serpentinization was studied by performing hydrothermal experiments at 400–500 °C and 3.0–20 kbar with natural ground olivine and peridotite as starting materials. Compared to olivine, peridotite is serpentinized at rates around 1–2 orders of magnitude faster. For experiments at 400–500 °C and 3.0 kbar with olivine as the starting material, < 1% of reaction extent was achieved after 19 days of serpentinization, which agrees well with previous experimental results (Martin and Fyfe 1970; Wegner and Ernst 1983; Malvoisin et al. 2012). In contrast, the kinetics of peridotite serpentinization are one–two orders of magnitude faster compared to the rates of olivine serpentinization, e.g., at 400 °C and 3.0 kbar and at 500 °C and 20 kbar, serpentinization reactions were completed within 20 days for peridotite with starting grain sizes of < 30 μm. The replacement of olivine by serpentine minerals was supported by FTIR analyses and observations under backscattered electron imaging. This is mainly attributed to the effect of pressure and the presence of pyroxene and spinel. Thermodynamic calculations show that Gibbs energy of olivine serpentinization decreases greatly with increasing pressure. Pyroxene minerals released some of their silica during the hydrothermal alteration of peridotite. The involvement of silica into serpentinization processes results in a more negative Gibbs energy of olivine hydrolysis with increasing pressures, and consequently the kinetics of peridotite serpentinization can be greatly enhanced.

Acknowledgements This work was financially supported by the Natural Science Foundation of China (41873069, 41603060), the Strategic Priority Research Program of the Chinese Academy of Sciences (XDA22050103, XDB42000000), and the National Key R&D Program of China (2016YFC0600408). We thank J. H. Zhu from the Second Institute of Oceanography, State Oceanic Administration of China for performing scanning electron microscope imaging. Thanks also to S. Jiang from South China University of Technology for the help during FTIR analyses. Supporting data are included in an SI file.

References

Allen DE, Seyfried WE Jr (2003) Compositional controls on vent fluids from ultramafic-hosted hydrothermal systems at mid-ocean ridges: an experimental study at 400 °C, 500 bars. Geochim Cosmochim Acta 67:1531–1542

Andreani M, Daniel I, Pollet-Villard M (2013) Aluminum speeds up the hydrothermal alteration of olivine. Am Mineral 98:1738–1744

Auzende AL, Daniel I, Reynard B, Lemaire C, Guyot F (2004) High-pressure behavior of serpentine minerals: a Raman spectroscopic study. Phy Chem Miner 31:269–277

Avrami M (1939) Kinetics of phase change. I General theory. J Chem Phys 7(12):1103–1112

Chen DG, Li BX, Zhi XC (1994) Genetic geochemistry of mantle-derived peridotite xenolith from Panshishan, Jiangsu. Geochimica 23:13–24

Costa IRD, Barriga FJAS, Viti C, Mellini M, Wicks FJ (2008) Antigorite in deformed serpentinites from the Mid-Atlantic ridge. Eur J Mineral 20:563–572

Dungan MA (1979) A microprobe study of antigorite and some serpentine pseudomorphs. Can Mineral 17:771–784

Escartín J, Hirth G, Evans B (1997) Effects of serpentinization on the lithospheric strength and the style of normal faulting at slow-spreading ridges. Earth Planet Sci Lett 151:181–189

Escartín J, Hirth G, Evans B (2001) Strength of slightly serpentinized peridotites: implications for the tectonics of oceanic lithosphere. Geology 29:1023–1026

Evans BW, Johannes W, Otterdoom H, Trommsdorff V (1976) Stability of chrysotile and antigorite in the serpentine multisystem. Schweiz Mineral Petrogr Mitt 56:79–93

Evans BW, Hattori K, Baronnet A (2013) Serpentinite: what, why, where? Elements 9:99–106

Foresti E, Gazzano M, Gualtieri AF, Lesci IG, Lunelli B, Pecchini G, Renna E, Roveri N (2003) Determination of low levels of free fibers of chrysotile in contaminated soils by X-ray diffraction and FTIR spectroscopy. Anal Bioanal Chem 376:653–658

Frost BR, Beard JS (2007) On silica activity and serpentinization. J Petrol 48:1351–1368

Fuchs Y, Linares J, Mellini M (1998) Mössbauer and infrared spectrometry of lizardite-1T from Monte Fico, Elba. Phys Chem Miner 26:111–115

Golightly JP, Arancibia ON (1979) The chemical composition and infrared spectrum of nickel and iron-substituted serpentine from a nickeliferous laterite profile, Soroako, Indonesia. Can Mineral 17:719–728

Guillot S, Hattori K (2013) Serpentinites: essential roles in geodynamics, arc volcanism, sustainable development, and the origin of life. Elements 9:95–98

Guillot S, Schwartz S, Reynard B, Agard P, Prigent C (2015) Tectonic significance of serpentinites. Tectonophysics 646:1–19

Hattori KH, Guillot S (2003) Volcanic fronts as a consequence of serpentinites dehydration in the fore-arc mantle wedge. Geology 31:525–528

Hébert R, Adamson AC, Komor SC (1990) Metamorphic petrology of ODP Leg 109, Hole 670A serpentinized peridotite: serpentinization processes at a slow spreading ridge environment. Proc ODP Sci Results 106(109):103–115

Hilairet N, Daniel I, Reynard B (2006) P-V equations of state and the relative stabilities of serpentine varieties. Phys Chem Miner 33:629–637

Hirth G, Guillot S (2013) Rheology and tectonic significance of serpentinite. Elements 9:107–113
Huang RF, Song MS, Ding X, Zhu SY, Zhan WH, Sun WD (2017a) Influence of pyroxene and spinel on the kinetics of peridotite serpentinization. J Geophys Res. https://doi.org/10.1002/2017JB014231
Huang RF, Sun WD, Zhan WH, Ding X, Zhu JH, Liu JQ (2017b) Influence of temperature, pressure, and fluid salinity on the distribution of chlorine into serpentine minerals. J Asian Earth Sci 145:101–110
Huang RF, Ding X, Lin CT, Zhan WH, Ling MX (2018) Effect of saline fluids on chlorine incorporation in serpentine. Solid Earth Sci 3:61–66
Huang RF, Sun WD, Song MS, Ding X (2019) Influence of pH on molecular hydrogen (H_2) generation and reaction rates during serpentinization of peridotite and olivine. Minerals. https://doi.org/10.3390/min9110661
Hyndman RD, Peacock SM (2003) Serpentinization of the forearc mantle. Earth Planet Sci Lett 212:417–432
Iyer K, Rüpke LH, Morgan JP (2010) Feedbacks between mantle hydration and hydrothermal convection at spreading centers. Earth Planet Sci Lett 296:34–44. https://doi.org/10.1016/j.epsl.2010.04.037
Iyer K, Rüpke LH, Morgan JP, Grevemeyer I (2012) Controls of faulting and reaction kinetics on serpentinization and double Benioff zones. Geochem Geophys Geosyst 13:Q09010. https://doi.org/10.1029/2012GC004304
Johnson JM, Oelkers EH, Helgeson HC (1992) SUPCRT 92: a software package for calculating the standard molal thermodynamic properties of minerals, gases, aqueous species, and reactions from 1 to 5000 bar and 0 to 1000 °C. Comput Geosci 18:899–947
Lafay R, Montes-Hernandez G, Janots E, Chiriac R, Findling N, Toche F (2012) Mineral replacement rate of olivine by chrysotile and brucite under high alkaline conditions. J Cryst Growth 347:62–72
Lafay R, Montes-Hernandez G, Janots E, Chiriac R, Findling N, Toche F (2014) Simultaneous precipitation of magnesite and lizardite from hydrothermal alteration of olivine under high-carbonate alkalinity. Chem Geol 368:63–75
Lamadrid HM, Rimstidt JD, Schwarzenbach EM, Klein K, Ulrich S, Dolocan A, Bodnar RJ (2017) Effect of water activity on rates of serpentinization of olivine. Nat Commun 8:16107
Liu XW, Liu XX, Hu YH (2014) Investigation of the thermal decomposition of talc. Clay Clay Miner 62:137–144
Malvoisin B, Brunet F, Carlut J, Rouméjon S, Cannat M (2012) Serpentinization of oceanic peridotites: 2. Kinetics and progresses of San Carlos olivine hydrothermal alteration. J Geophys Res 117:B04102. https://doi.org/10.1029/2011JB008842
Marcaillou C, Muñoz M, Vidal O, Parra T, Harfouche M (2011) Mineralogical evidence for H_2 degassing during serpentinization at 300 °C/300 bar. Earth Planet Sci Lett 303:281–290
Martin B, Fyfe WS (1970) Some experimental and theoretical observations on the kinetics of hydration reactions with particular reference to serpentinization. Chem Geol 6:185–202
McCollom TM, Bach W (2009) Thermodynamic constraints on hydrogen generation during serpentinization of ultramafic rocks. Geochim Cosmochim Acta 73:856–875
McCollom TM, Frieder K, Robbins M, Moskowitz B, Berquó TS, Jöns N, Bach W, Templeton A (2016) Temperature trends for reaction rates, hydrogen generation, and partitioning of iron during experimental serpentinization of olivine. Geochim Cosmochim Acta 181:175–200
Nakatani T, Nakamura M (2016) Experimental constraints on the serpentinization rate of fore-arc peridotites: implications for the upwelling condition of the slab-derived fluid. Geochem Geophys Geosyst 17:3393–3419
O'Hanley DS (1996) Serpentinites: records of tectonic and petrologic history. Oxford University Press, New York, pp 217
O'Hanley DS, Chernosky JV Jr, Wicks FJ (1989) The stability of lizardite and chrysotile. Can Mineral 27:483–493
Peacock SM (2001) Are the lower planes of double seismic zones caused by serpentine dehydration in subducting oceanic mantle? Geology 29:299–302
Rüpke LH, Morgen JP, Hort M, Connolly JAD (2004) Serpentine and the subduction zone water cycle. Earth Planet Sci Lett 223:17–34
Saumur BM, Hattori KH, Guillot S (2010) Contrasting origins of serpentinites in a subduction complex, northern Dominican Republic. GSA Bull 122:292–304
Scambelluri M, Rampone E, Piccardo GB (2001) Serpentinite: a trace-element study of the Erro-Tobbio high-pressure ultramafites (Western Alps, NW Italy). J Petrol 42:55–67
Scambelluri M, Fiebig J, Malaspina N, Müntener O, Pettke T (2004) Serpentinite subduction: implications for fluid processes and trace-element recycling. Int Geol Rev 46:595–613
Schmidt MW, Poli S (1998) Experimentally based water budgets for hydrating slabs and consequences for arc magma generation. Earth Planet Sci Lett 163:361–379
Schwartz S, Guillot S, Reynard B, Lafay R, Debret B, Nicollet C, Lanari P, Auzende AL (2013) Pressure-temperature estimates of the lizardite/antigorite transition in high pressure serpentinites. Lithos 178:197–210
Seyfried WE Jr, Dibble WE Jr (1980) Seawater-peridotite interaction at 300 °C and 500 bars: implications for the origin of oceanic serpentinites. Geochim Cosmochim Acta 44:309–321
Seyfried WE Jr, Foustoukos DI, Fu Q (2007) Redox evolution and mass transfer during serpentinization: an experimental and theoretical study at 200 °C, 500 bar with implications for ultramafic-hosted hydrothermal systems at mid-ocean ridges. Geochim Cosmochim Acta 71:3872–3886
Sun WD, Peng ZC, Zhi XC, Chen DG, Wang ZR, Zhou XH (1998) Osmium isotope determination on mantle-derived peridotite xenoliths from Panshishan with N-TIMS. Chin Sci Bull 43:573–575
Ulmer P, Trommsdorff V (1995) Serpentine stability to mantle depths and subduction-related magmatism. Science 268:858–861
Wallmann K (2001) The geological water cycle and the evolution of marine delta O-18 values. Geochim Cosmochim Acta 65:2469–2485
Wegner WW, Ernst WG (1983) Experimentally determined hydration and dehydration reaction rates in the system MgO-SiO_2-H_2O. Am J Sci 283-A:151–180
Wicks FJ, Whittaker EJW (1977) Serpentine textures and serpentinization. Can Mineral 15:459–488
Wood BJ, Walther JV (1983) Rates of hydrothermal reactions. Science 222:413–415
Wu K, Ding X, Ling MX, Sun WD, Zhang LP, Hu YB, Huang RF (2018) Origins of two types of serpentinites from the Qinling orogenic belt, central China and associated fluid/melt-rock interactions. Lithos 302–303:50–64
Xia Y, Ding X, Song MS, Xiong XL, Shao TB, Li JF, Hao XL (2014) Temperature determination and thermal structure analysis on the pressure assembly of a piston-cylinder apparatus. Chin J Phys 28:262–272
Xu XS, Griffin WL, O'Reilly SY, Pearson NJ, Geng HY, Zheng JP (2008) Re-Os isotopes of sulfides in mantle xenoliths from eastern China: progressive modification of lithospheric mantle. Lithos 102:43–64
Yang XY (2008) Geochemical study on Cenozoic mantle derived peridotitic xenoliths from Panshishan and Lianshan, Jiangsu Province. Dissertation, University of Chinese Academy of Sciences